the general science journal

Fifty Years of Liquid Phase Photodeposition Research Progress

Aaron Peled and Simona A. Popescu

Photonics Laboratory, Electrical and Electronics Engineering Faculty,
Holon Institute of Technology, Holon, Israel
Email: peledd@gmail.com

Abstract

Liquid Phase Photo Deposition (LPPD) is a thin-film deposition method where photosensitive colloidal precursors in suspension are deposited onto transparent substrates by optical excitation, essentially a photonic analogue of electrodeposition. Pioneered with amorphous selenium (a-Se), the method's kinetic and theoretical foundations include photo-adsorption and light-induced colloidal aggregation. Subsequently it was extended to CdS, ZnS, and bio-chromophore colloids, establishing photo-induced precursor destabilization as a general thin film-growth mechanism. Applications span optical recording, holographic gratings, reversible write/erase cycles, archival holography, and diffractive optical elements via mask, direct-write, or computer-generated holographic exposure. Recent advances included pulsed excimer-laser excitation and real-time evanescent-field imaging. The review compares it to other related processes such as photocatalytic deposition, photo-assisted CVD, and photo-assisted electrodeposition.

Keywords: photodeposition, thin films deposition, colloids, nanoscopic layers.

1. Introduction

The term photodeposition emerged from experiment rather than theory. In the late 1970s, collaborators at the Hebrew University of Jerusalem discovered that illuminated colloidal hydrosols of amorphous selenium (a-Se) could deposit thin solid films onto immersed transparent substrates. The name was coined by analogy with electrodeposition. As electrical current drives ion deposition, light drives material deposition onto a surface. In both cases, an external stimulus destabilizes a dispersed precursor and directs it onto a surface. This principle became the foundation of Liquid Phase Photodeposition (LPPD). The discovery was first presented at the Israel Physical Society meeting (Technion, Haifa, April 1976) and at the Electrochemical Society Annual Meeting (Philadelphia, May 1977). It was later formalized in a three-part archival study in Thin Solid Films (1978), establishing the structural, kinetic, and theoretical foundations of the "Selor Process".

This review covers the light-driven deposition LPPD of thin films and nanostructures from colloidal or dispersed liquid-phase systems onto solid substrates. Initiated by Perakh and Peled

(1976–1978), the field developed over five decades through international collaborations spanning thin-film physics, holographic recording, diffractive optics, nanoscale fabrication, and evanescent-field optical metrology. This review draws primarily on the Peled group's publications from 1978 to 2020 [1–53], with additional external references [54–71] for comparison and related context.

2. Defining Liquid Phase Photodeposition (LPPD)

Liquid Phase Photodeposition (LPPD) is a controlled, light-driven deposition of solid material from a colloidal hydrosol or dispersed liquid-phase system onto a solid substrate surface. In the a-Se case, the basic ingredients are selenious acid H_2SeO_3 and sodium sulfite Na_2SO_3, which generate the initial selenium nuclei seeds in the hydrosol in the dark according to the chemical reaction:

$$H_2SeO_3 + 2Na_2SO_3 \xrightarrow{dark,\ then\ h\nu \geq 2eV} Se + 2Na_2SO_4 + H_2O$$

In the next step, a transparent electrically insulating substrate is immersed in the hydrosol perpendicular to the beam axis. Upon illumination, the selenium seeds act as a visible-UV photocatalyst ($E_{gap} = 2$ eV). Sodium sulfite serves as a sacrificial hole scavenger, promoting autocatalytic growth of the selenium particles in the hydrosol. The colloid then destabilizes along the beam axis within an elongated volume whose cross-sectional geometry conforms to the beam profile at each point along its propagation axis. Consequently, more amorphous selenium precipitates and deposits onto the substrate surface, more strongly on the back surface, providing a spatially and temporally controlled deposition process. The smallest newly formed Se particles agglomerate near the illuminated substrate and adsorb there by van der Waals forces, producing the orange-red photodeposited a-Se thin film. The photodeposition reactor system is illustrated in Fig. 1.

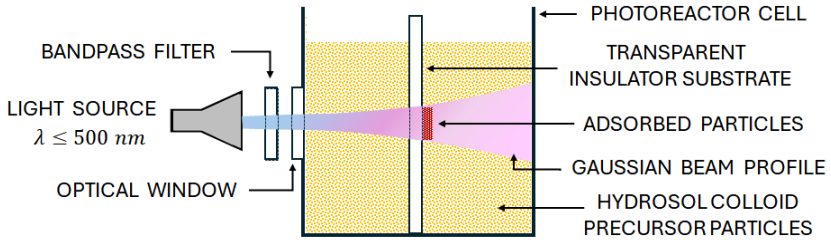

Fig. 1. Schematic drawing of the photoreactor showing the main components.

The resulting deposit is ideally a smooth, mirror-like thin film. Alternatively, when initial conditions are not perfect, a more frustrated structured layer may form instead. In either case, the thickness, microstructure, and optical properties of the deposited layer are governed by two sets of factors. The first set relates to the illumination conditions: wavelength, intensity, and duration. The second set relates to the colloid properties: particle size, concentration, surface rheology, and temperature. The colloidal nature of the precursor is central to the process, not merely incidental. Colloidal particles occupy a nanometer-to-micrometer size regime. Within this regime, stability is governed by a balance of surface forces, van der Waals interactions, and electrostatic double-layer repulsion. Upon excitation, several coupled effects can trigger modifications to the particles charge-carrier populations, alter surface potentials,

induce heating of the hydrosol leading to aggregation behavior, and change particle rheology. This dependence on both material and illumination parameters gives LPPD its tunability. LPPD is also not limited to a single material system i.e., selenium. In principle, any metastable colloidal suspension with sufficient optical absorption and photo-responsive stability may serve as an LPPD precursor. Over five decades, this generality has been demonstrated across a-Se, CdS, ZnS, and bio-chromophore systems [3–5, 20, 27, 36].

Within LPPD itself, two photoactivated modes were identified. In surface photodeposition, illumination is directed at the substrate surface, so deposition occurs preferentially at the illuminated region. This enables patterned writing on transparent substrates, with resolution limited by the optical system focus and particles size [15, 24, 25]. In volume photodeposition, illumination of the colloid hydrosol induces precipitation in the bulk, and the particles subsequently settle at the bottom of the photoreactor. The two modes share the same basic physics but differ in geometry, kinetics, and application.

3. The Founding Selor Process of a-Se (1976–1989)

3.1 Structure, Kinetics and Interpretation

The first systematic experimental investigations of LPPD were published in 1978 in a trilogy of papers [3–5] in *Thin Solid Films* by M. Perakh et al. These introduced the process as the "Selor" Process, a name reflecting its selenium-based origin and light excitation of the hydrosol. The first paper [3] outlined the main structural features of the process and its deposited films. Structural characterization confirmed the amorphous nature of the deposits and revealed that film morphology was controlled by light intensity and exposure duration. The second paper [4] focused on the kinetics of photodeposition. Measurements of deposition rates as functions of illumination intensity, colloid concentration, and temperature revealed that the process followed well-defined kinetic laws, with distinct induction, growth, and saturation phases. The photodeposition experiments described in references [3-6] were conducted on Polyethylene Terephthalate (PET) and Polymethyl Methacrylate (PMMA) substrates within a temperature range of 0-25°C, utilizing a mercury discharge lamp equipped with narrow-band filters for spectral line selection in the 400–600 nm region. Experimental results indicated that the best film quality deposition was achieved using the 435 nm blue spectral line. In the extensive experimental procedures, the light intensity was varied from 0 to 53 μW/cm², with incubation times corresponding to 2-9 hours. The kinetics of the process were notably temperature-dependent. At 15°C, the Quasi-Linear Deposition Rate (QLDR) was approximately 4 nm/sec, whereas at 5°C, it decreased to 1.34 nm/sec. The calculated activation energy for the process ranged from 2 to 14.6 kcal/mol, varying according to the specific photoexcitation states involved.

Morphological analysis via Scanning Electron Microscope (SEM) [3] showed that the adsorbed particle diameters on PET substrates ranged from 0.05 to 0.7 μm for deposition times of 5-20 hours corresponding to temperatures between 5°C and 15°C. At the beginning of the photodeposition, discrete particles/drops are adsorbed onto the substrate surface see Fig. 2a. At longer irradiation times they grow and coalesce as seen in Fig. 2b showing a photodeposited film at the border between a compact film (left) and a yet unaggregated zone of discrete particles (right).

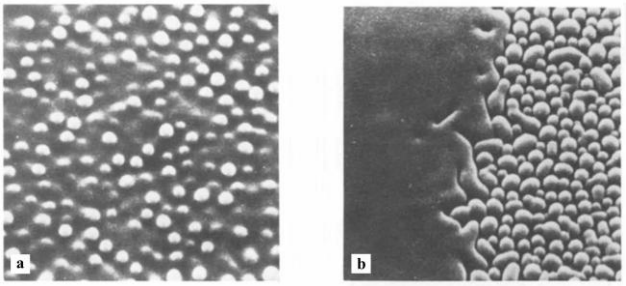

Fig. 2. SEM micrographs of photodeposited amorphous selenium a) initial discrete particles/drops deposited on the substrate, magnification x9600 b) the border between a compact film and an area with uncoalesced particles, magnification x12000.

The final film thicknesses were obtained in the range of ~ 0.5-1.5 μm as determined by transmission densitometry using the 546 nm mercury line, which was selected for its optimal signal-to-noise ratio and high sensitivity to thickness variations. Paper [5] provided also a theoretical interpretation of both the structural and kinetic observations. It proposed a model in which photo-excitation of selenium colloid particles modifies their surface energy and interparticle interaction potentials, reducing the barrier to adhesion at the substrate surface. This 1978 interpretive framework anticipated the more elaborate theoretical developments that would emerge over the following decade for LPPD.

3.2 Light–Temperature Interference and Photo-adsorption

A significant conceptual realization occurred in 1979 with the investigation of light–temperature assisted combined effects governing the photo-adsorption and photodeposition of a-Se films [6]. This and subsequent studies revealed that the relationship between illumination and deposition was not purely photonic. Instead, the underlying physics proved more complex, with both photonic and thermal influences simultaneously governing the LPPD process, as evidenced by an observed isokinetic (compensation) temperature of ~303 K, to be discussed further [6,53].

3.3 Hydrosol Properties and Volume Photodeposition Details

By the mid-1980s, the colloidal precursor medium itself had become the subject of study in Papers [7,8], which examined a-Se hydrosols in the dark. Particle size distributions, stability, and rheological behavior were characterized as baseline properties of the metastable colloid, providing the reference conditions needed to measure photo-induced changes precisely. Optical turbidity measurements analyzed the metastable hydrosol properties of the Standard a-Selenium Hydrosol stored at 5°C yielding a typical particle concentration $N \sim 6.73 \times 10^{11}$ cm^{-3} with an Effective Particle Diameter of 26 nm. These values were obtained by measuring the Specific Turbidity (τ/C) and applying the Rayleigh approximation [7]. The small diameter found at this temperature supports the hypothesis that the particles exist in a "near embryo state" in the dark, only reaching full growth once photoactivated. Paper [8] then characterized optically the volume photodeposition, in which illumination is distributed throughout the bulk of the colloid rather than confined to the substrate surface. Under these conditions, particles throughout the solution are destabilized, leading to photo-precipitation and material settling, mainly at the bottom of the photoreactor. The various fundamental photodeposition processes

and photoreduction in colloidal solutions upon irradiation were detailed in [23] and are illustrated here in Fig. 3.

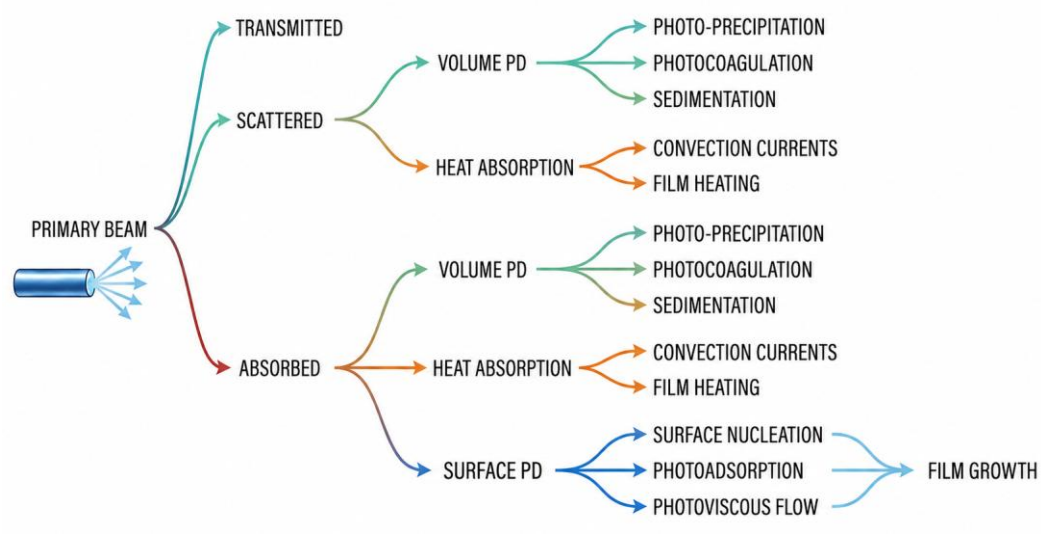

Fig. 3. Schematic of the various processes during photodeposition activated by the illumination

3.4 Recording, Display Technology and Early Applications

The potential of LPPD for optical recording and display applications was first reported in 1985 [9]. The study examined the main recording parameters, including photosensitivity, resolution, photographic dynamic range, and the stability of the photodeposited a-Se films as a recording medium. In that study, Surface Photodeposition (SP) exhibited a response time of approximately 3 hours when exposed to a mercury discharge light with bandpass filtered wavelength at 435 nm and an irradiance of 50 μW/cm². This could be reduced to a matter of seconds by using an Argon CW laser line (458 nm) with a much higher irradiance of ~ 1.5 W/cm² [21]. Then even shorter times of ~ 350 nsec were obtained using a KrF pulsed laser (248 nm) [46] with cumulative fluence of ~ 1.8 J/cm² and finally 100 nsec with an ArF pulsed excimer laser (193 nm) [45] with a cumulative fluence of ~ 200 mJ/cm². The line resolution was in the 2.5-5 μm range for films with thickness 2 μm. In contrast, Volume Photo-precipitation (VP) demonstrated significantly faster turbidity - τ response times, ranging from 1 second for C = 0.06 M concentration of the Se hydrosol to 1 nsec for C = 0.24 M Selenium, following an empirical relationship $\tau = \tau_0 \exp(bC)$ [9]. These results placed LPPD within the broader field of optical recording technologies which were under active development then. Liquid-phase processing, room-temperature operation, and direct optical patterning without photoresist intermediates outlined the distinct advantages of LPPD over the solid state more complex photoresist-based recording methods.

3.5 Electrical, Photoelectrical and Optical Properties of Deposited Films

A comprehensive characterization of the electrical and photoelectrical properties of photodeposited a-Se films was published in 1985 [10]. Measurements of dark conductivity, photoconductivity, and carrier mobility showed that the films had semiconducting properties consistent with amorphous selenium, and that these properties could be modified by post-thermal processing. Electrical characterization of the resulting films showed a dark conductivity of 10^{-11} to $10^{-10}\Omega^{-1}cm^{-1}$ at room temperature. The photoelectrical response

was also examined for detector applications. Photocurrent measurements of the photodeposited films showed a power-law of the form $\Delta I_{ph} \propto H^{\gamma}$ with $\gamma \approx 0.82$.
This indicates an amorphous state. Hence in the original photodeposited a-Se, the transport is dominated by a broad distribution of localized states (traps) in the bandgap. The post thermal treatment induces crystallization of a-Se into the stable trigonal (hexagonal) form. In this crystalline state, the disordered "tail states" are removed, and the recombination kinetics simplify to $\gamma \sim 0.5$ which is the signature of pure bimolecular recombination.

In 1986 [12], the optical properties of photodeposited a-Se films were characterized in detail, including the refractive index, absorption coefficient, and optical bandgap as functions of film thickness and deposition conditions. The results showed optical quality comparable to films produced by conventional vacuum deposition methods, which are more expensive and hazardous. The optical absorption constant α, absorption index k and refractive index n were similar to those reported in the literature for a-Se in the wavelength range of 400-650 nm. The optical bandgap of $E_G \approx 2.05$ eV was also in agreement with results of vacuum deposited films.

X-ray fluorescence analysis [11] complemented these studies by determining impurity content and confirming the chemical purity of the films, addressing concerns about processing contamination from the liquid-phase. Based on X-ray fluorescence measurements, the impurity levels showed in fact a marked decrease as the process progressed from the raw reagent materials used to the final photo-precipitated product. Starting with initial reagents impurity concentrations like Iron (Fe), Zinc (Zn), Copper (Cu), and Chromium (Cr) of ~ 10^{-4} % w/o, during dark precipitation and photodeposition, their values were reduced to about 10^{-6} % w/o. (Note : 10^{-4} % w/o = 0.0001 weight percent of impurity).

3.6 Phenomenological Initial Kinetic Models

The theoretical foundation of LPPD was initiated by two studies published in 1987 and 1988. Paper [13], co-authored with D. Naot, introduced a phenomenological model of photo-precipitation in a-Se colloid solutions, describing the photo-induced transition from a metastable colloid to a depositing system through modified interaction potentials and barrier energetics. It provided a quantitative framework for predicting the onset and rate of photodeposition as a function of illumination and colloid parameters and introduced the concept of a photo-precipitation threshold, defined as the critical illumination intensity above which deposition starts. Paper [14] developed a complementary kinetic model of photo-adsorption from a-Se colloids, deriving expressions for the parameters governing the initial adsorption stage of photodeposition. The model identified the key rate-determining steps and their dependence on temperature and light intensity, and presented a simple, physically transparent mathematical framework that could also apply to other colloidal photodeposition systems beyond a-Selenium.

3.7 Equations of the Phenomenological Kinetics Model

During a-Se Photodeposition three main time regimes are observed quite generally with 2 time constants τ_1 and τ^* discussed extensively in Paper [14]:

(a) Incubation period for $0 < t < \tau_1$

(b) Quasi-linear growth period for $\tau_1 < t < \tau^* + \tau_1$

(c) Saturation for $t > \tau_1 + \tau^*$

The phenomenological thickness-time relationship is fitted to the experimental Surface Photodeposition data which follows best a Logarithmic Film Growth Law:

$$\xi(t) - \xi_1 = \kappa \cdot \ln\left(\frac{t-\tau_1}{\tau^*} + 1\right) \text{ [cm]} \qquad (1)$$

where: $\xi(t)$ is the film thickness at time t, ξ_1 is the film thickness at the onset of the quasi-linear growth ($t = \tau_1$) and κ is the characteristic thickness parameter defined by the quasi-linear period. Altogether the 4 fitting parameters are obtained from Eq. (1) by least-squares regression. The time derivative of Eq. (1), gives the instantaneous deposition film growth rate:

$$\frac{d\xi}{dt} = \frac{\kappa}{\tau^*} \cdot \exp\left(\frac{\xi_1}{\kappa}\right) \cdot \exp\left(-\frac{\xi(t)}{\kappa}\right) \text{ [cm/sec]} \qquad (2)$$

where $d\xi/dt$ is the instantaneous film growth rate at thickness $\xi(t)$.

The growth rate peaks at $t = \tau_1$ with the characteristic ratio κ/τ^*, so called initial quasi linear growing rate. This growth rate decays exponentially as the film thickens due to increased optical absorption in the growing film. In terms of the flux of the colloid particles arriving at the substrate surface, i.e., we have a particles current density form of Eq. (2) given by:

$$J_p(t) = f \cdot \frac{\kappa}{\tau^*} \cdot \exp\left(\frac{\xi_1}{\kappa}\right) \cdot \exp\left(-\frac{\xi(t)}{\kappa}\right) \left[\frac{\text{particles}}{\text{cm}^2 \cdot \text{sec}}\right] \qquad (3)$$

where: J_p is the particle current density at the substrate at time t, f is a conversion factor relating the film growth rate $d\xi/dt$ to the flux density of colloidal particles depositing per unit area per second.

The particle current density originates from the Smoluchowski equation, which governs diffusive transport in the presence of an external potential. (Basically, stemming from Fick Law: $J = D\frac{dc}{dx}$, where c is the concentration of the diffusing particles).

By using a step potential approximation: $U(x) = U_0$ for $0 \le x \le x_{\text{eff}}$ we get:

$$J_{ps} = \frac{Se^*_{max} \cdot D}{W} \left[\frac{1}{\text{cm}^2 \cdot \text{sec}}\right] \qquad (4)$$

where $W = \int_0^{x_{\text{eff}}} e^{U(x)/kT}\, dx = x_{\text{eff}}\, e^{U_0/kT}$ and Se^*_{max} is the maximum concentration of photo-excited Se colloid particles in the adsorption zone. D is the diffusion coefficient of the excited Se* particles concentration in the volume, k is the Boltzmann constant, and T temperature. $U(x)$ is the position-dependent potential energy (screening barrier) approximated by $U_0 \approx 0.258\, eV$. $x_{\text{eff}} \approx x_D = \sqrt{D \cdot \tau_D}$ is the effective liquid layer over which the photo-adsorption potential acts and is approximated here by the diffusion length x_D of the colloid particles near the surface.

Note that Eq. (4) connects the measurable macroscopic deposition current to the microscopic barrier potential U_0 and the diffusion properties of the colloid, providing a physical model for the empirical parameters in Eq. (1) and (2).
Simulations for various temperature conditions such as T ≈ 300 K, a constant photon flux of 3.2×10^{14} photons cm^{-2} s^{-1} at λ = 435 nm, mean colloid radius of r_m = 15 nm, diffusion coefficient $D = 1.4 \times 10^{-7}\ cm^2/sec$, screening barrier $U_0 \approx 0.258$ eV, and a maximum colloid concentration $Se^*_{max} \sim 2 \times 10^{13}\ cm^{-3}$ were carried out. Using the above parameters, the model gives a typical film-growth rate of about $6.2 \times 10^{-9}\ cm/sec$ for the photodeposition process [14].

3.8 Microstructural Evolution and Low-Temperature Photodeposition

The microstructural evolution of photodeposited a-Se films as a function of thermal and aging conditions was examined in 1989 [17], revealing a sequence of plastic transformation steps. The process begins with an amorphous deposited state, which, upon heating, transitions through intermediate metastable configurations toward crystalline phases, with the specific pathways highly sensitive to thermal treatment conditions. This phase of LPPD research concluded with a thermal characterization study conducted with E. Hadziioannou in 1991 [18]. The work expanded the parameter space of the Selor Process to include conditions of reduced thermal activation. It demonstrated that compact films could be obtained at significantly lower temperatures than previously achieved, and that the properties of these films differed from those deposited at higher temperatures.

4. Kinetics and Thermodynamics Modeling

4.1 Photo-adsorption Kinetics and the Compensation Effect

A 1988 study [16] extended the framework of [14] by examining the thermal surface activation energy in photo-adsorption kinetics, placing LPPD within the broader class of thermally activated processes. In Papers [14, 16], photo-adsorption, the stage in which photo-excited colloid particles adsorb onto the substrate before continuous film formation, was modeled as a thermally activated process in which illumination alters the effective activation barrier through photo-induced changes in particle surface energy. Paper [16] identified a compensation effect consistent with the Meyer-Neldel rule, in which the logarithm of the pre-exponential factor varies linearly with the activation energy, an effect seen also in semiconductors intrinsic carrier concentration and in the mobility temperature dependence of Molecularly Doped Polymers (MDP) (see [53]). This suggested that the photodeposition rate-determining step reflects a coupled photon-temperature interaction at the colloid-substrate interface rather than a simple photon-driven unimolecular surface event. The isokinetic temperature was found at T*~303K which locates this peculiar compensation behavior of the deposition rate near room temperature.

4.2 Aggregation Kinetics by Photon Correlation Spectroscopy

A complementary perspective on LPPD dynamics was provided by the study of the aggregation kinetics in photo-excited colloid solutions using Dynamic Photon Correlation Spectroscopy (PCS), reported in Paper [28] (1995). Unlike approaches that monitor deposition

at the substrate surface, this study focused on the evolution of particle size distributions in the colloid hydrosol itself under illumination, investigating the aggregation precursor stage that precedes surface deposition. PCS measurements revealed that photo-excitation induced progressive aggregation of a-Se particles across two distinct temporal regimes. In the particles growth regime ($t < 10^3\ sec$), both mean diameter and scattered intensity follow power laws like $\varphi(t) = \varphi_0 \cdot t^{\mathrm{n}}$ and $I(t) = I_0 \cdot t^{\mathrm{l}}$, respectively reflecting an out-of-equilibrium, kinetically driven aggregation process with dose-dependent exponents n and l. In the saturation regime ($t \geq 1500\ sec$), both parameters reach stable, dose-dependent plateau values, indicating colloid re-stabilization through interparticle repulsion or steric effects. This appears as a dose-memory effect in which the system freezes into a final state set by the irradiation dose delivered. These kinetics are consistent with a diffusion-limited cluster aggregation model modified by photo-induced reduction of the interparticle repulsion barrier. This study provided thus a microscopic experimental window into the volume colloidal growing physics underlying LPPD, complementing the macroscopic kinetic descriptions presented in Papers [4], [14], and [16].

4.3 Optical Response Properties of Irradiated Colloid Systems

The theoretical description of the optical response of the photoexcited colloid system, specifically, how the optical properties of the suspension evolve in its photoreactor volume, was first addressed in Paper [32] (1996). In this paper an expression for the optical absorption constant $\alpha(x,t)$ in an irradiated colloidal system undergoing photo-precipitation was developed. Starting from coupled partial differential equations governing light intensity, photoexcitation, and precipitation dynamics, an analytical result was developed for $\alpha(x,t)$ that captures two competing mechanisms at play:

$$\frac{\alpha(x,t)}{\alpha_0} = e^{-A}\exp(kI_0t)\,; \qquad A = \sum_{n=1}^{\infty} \frac{x^n(\alpha^n - \alpha_0^n)}{n \cdot n!}$$

A is a dimensionless spatial attenuation series summed over integer orders n = 1, 2, 3, ..., with x the spatial coordinate measured from the irradiation window. I_0 is the constant light intensity at the window entrance, $\alpha(x,t)$ is the local optical absorption constant, and α_0 its initial value in the medium. Each term of order n contributes a correction proportional to the spatial displacement x^n and the deviation $\alpha^n - \alpha_0^n$ from the initial state, weighted by the factorial factor $n \cdot n!$. Physically, A represents the cumulative spatial screening of light at position x within the medium. It quantifies how much the local optical absorption has deviated from its initial optical value α_0 as photo-precipitation progresses, essentially measuring the accumulated optical obstruction built up at distance x due to the growing concentration of newly created chromophores. The factor $exp(kI_0t)$ represents the positive autocatalytic feedback driven by photo-precipitation, while e^{-A} encodes the self-screening negative feedback that suppresses light penetration into the bulk. The linearized form of this result yields a well-defined propagation velocity $v = x/t = kI_0/(\alpha - \alpha_0)$ for the photoexcitation front wave propagating through the medium. The numerical results confirm that $\alpha(x,t)$ amplification is practically unlimited only within a thin layer of characteristic thickness $0.1/\alpha_0$ near the irradiation window, beyond which screening dominates. These findings are consistent

with the experimental observations and have direct implications for the design of the photoreactor system, where the active photo-precipitation zone is inherently confined to the vicinity of the entrance window.

4.4 Visualization and Simulation of Thin Film Growth

The final theoretical contribution of this LPPD research strand focused on the visualization and simulation of thin film growth during photodeposition, as detailed in Papers [35] and [40]. In Paper [35] (2000), a simulation framework was introduced to model thin film growth, where particle adhesion to the substrate is governed by local surface coverage and illumination intensity. The method encodes the evolving surface morphology as a two-dimensional image density function φ(x, y, t), sampled from scanning electron microscopy (SEM) micrographs of amorphous selenium (a-Se) particles or constructed synthetically as Gaussian spheroid arrays. Physical driving forces, surface diffusion, material deposition, desorption, and lateral translation, are unified into a single spatio-temporal partial differential equation (PDE).

$$\partial\varphi/\partial t + \nabla(\bar{v}\varphi) - D\,\nabla^2\varphi + \alpha\varphi = f$$

where D is the diffusion coefficient governing material spreading across the substrate, α is a deposition/absorption coefficient (negative for desorption), $\bar{v}$ is a translation velocity, and f is a general time-dependent source photodeposition term.

Rather than solving this equation by computationally expensive real-space convolution, the framework transforms both the image and the PDE into the 2D Fourier spatial frequency domain $\bar{\omega}$, where temporal evolution reduces to pointwise multiplication by an analytic transfer function $S(\bar{\omega}, t)$. For the diffusion-deposition model, $S(\bar{\omega}, t)$ takes the form of a time-dependent Gaussian low-pass filter whose cutoff narrows as diffusion progresses, directly mirroring the physical smoothing of the fine particle detail. The study captured key surface morphology features, including particle adsorption, island coalescence, and the transition from discontinuous to continuous film coverage. Notably, the simulated film morphologies align with the experimentally observed microstructures (see Fig. 4).

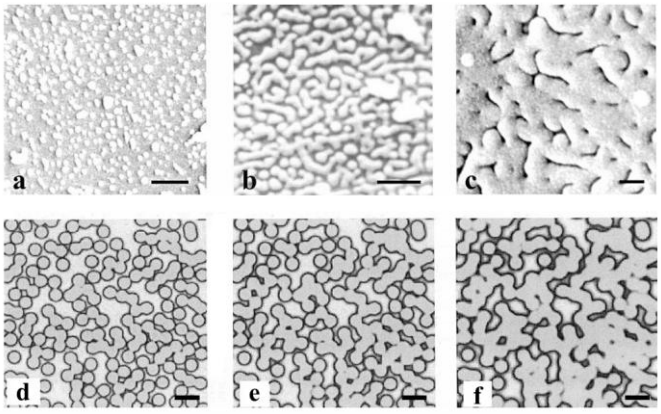

Fig. 4. Comparison of scanning electron microscopy (SEM) micrographs (a–c) with corresponding computer-simulation results (d–f). The images illustrate the evolutionary stages of photodeposited particles, from isolated particle adsorption to bridging and coalescence during film formation of a monolayer. Scale bars correspond to 5 μm in (a), 2 μm in (b), and 0.5 μm in (c–f).

5. Materials Gamut Expansion

LPPD is a fundamental process based on photo-induced colloidal destabilization. The same phenomenon also occurs in other suspensions in which particles absorb enough optical energy to disrupt hydrosol metastability. This broader applicability has been confirmed through investigations of the following materials.

5.1 CdS Colloids and Photodeposition of Cadmium Films

The first extension of LPPD beyond a-Se was reported in 1992 in Paper [20], co-authored with Weiss and Friesem of the Weizmann Institute of Science. The collaboration combined LPPD expertise developed over the preceding decade with holographic and optical material capabilities and applied the method to the cadmium sulfide system because of its optical properties and established role as a photosensitive semiconductor. The study showed that chemically prepared CdS colloid solutions, under illumination from laser or discharge lamps at wavelengths shorter than about 514 nm, could deposit black, cadmium-rich thin films onto immersed substrates. The quantum yield of the photodeposition process increased by several orders of magnitude from visible 514 nm light to UV 366 nm irradiation. Because cadmium-based thin films have optical and electronic properties of interest for detectors and recording applications, the LPPD route opened a new ambient-condition patterning method for this material, bypassing vacuum-based thin-film processing.

5.2 ZnS Colloid Solutions and Laser-Induced Photodeposition

The extension to zinc sulfide colloids was reported in a 1995 paper [27]. The study examined laser-induced photodeposition from ZnS colloid solutions, by focused KrF laser illumination at 248 nm to drive localized deposition from the colloidal medium. The introduction of laser excitation added a new degree of spatial control to the LPPD process. The high intensity and precise spatial definition of the laser beam allowed ZnS deposition to be confined to sub-millimeter regions of the substrate surface, with lateral resolution determined by the beam diameter and by the nonlinear dependence of the deposition rate on illumination intensity. This spatial selectivity, together with the chemical versatility of ZnS as a wide-bandgap semiconductor, showed that laser-induced LPPD could serve as a direct-write fabrication tool capable of producing patterned thin-film structures from a liquid-phase precursor without lithographic masking or resist processing.

5.3 Chlorophyll-Based Bio-Chromophore Solutions

A 2000 study in Paper [36], co-authored with Y. Dror et al., extended LPPD to chlorophyll-based solutions documented photobleaching and photodeposition processes under UV and visible illumination. As a biological pigment straddling true molecular solutions and colloidal dispersions, chlorophyll blurs the line between photochemical reaction and colloidal photodeposition, a qualitative departure from the prior inorganic systems. A companion paper [41] by N. Mirchin et al. (2003) provided a quantitative model of the bleaching kinetics. Together, these works bridged classical inorganic LPPD with bio-photonics and bioinspired materials.

5.4 Comparison of Film Morphology Across the Investigated Materials

The morphological outcomes of LPPD reflect each material's intrinsic physical properties. In amorphous selenium, photo-induced viscous plasticity enables cooperative coalescence. Droplets nucleate and merge into a continuous, low-volume phase, yielding a specular, mirror-like finish [3, 17, 18, 29]. CdS and ZnS, by contrast, form frustrated aggregates since their rigid, brick-like particles cannot coalesce smoothly, producing stochastic porous networks and matte, scattering surfaces [20, 27]. Chlorophyll presents yet another limitation: steric and viscous barriers favor fibrous, convection-patterned deposits over planar films [36, 41, 52]. Preliminary experiments with gold, crystalline hexagonal-Se, and elemental sulfur failed to produce the metastable, photo-excitable colloidal state required for thin-film deposition, indicating that photosensitivity alone is insufficient. Taken together, these results reveal a material filter governing film quality. Beyond the universal LPPD architecture, i.e., a precursor, a photon, and a substrate, a smooth, specular film requires a material that is also structurally plastic, amorphous, low-T_g, or otherwise viscous enough to relax many-body packing constraints during and after deposition [35]. A lustrous, continuous thin film thus appears to be a privilege of materials capable of liquid-like coalescence on the substrate.

6. Photonics Applications I : Optical Recording and Holography (1988–1997)

6.1 Using LPPD for Planar Photonic Devices

By the late 1980s, the structural, kinetic, and theoretical foundations of the Selor process had been established across a series of studies on a-Se [3–18], and the material properties of photodeposited films, including optical quality, refractive index, absorption coefficient, and photoelectrical response, had been shown to be similar to those of films produced by conventional vacuum methods [10–12]. The stage was then set for the systematic exploration of LPPD as a fabrication platform for photonic devices and recording media. The key enabling insight was spatial controllability. Because LPPD deposition at every point on the substrate is driven by local illumination intensity, any structured light field, whether a focused beam, an interference pattern, or a holographic reconstruction, translates directly into a corresponding spatial pattern of deposited material.

6.2 Optical Photorecording by Surface Photodeposition

Paper [15] from 1988 gave the first explicit demonstration of optical recording by LPPD. A substrate, serving also as an optical window, was placed in contact with an a-Se hydrosol and illuminated from its dry side (non-immersive mode). This produced surface deposits whose thickness and optical density tracked the local intensity distribution. The result was a directly written optical record requiring no development or photoresist processing. The colloidal suspension itself served as the recording medium, with the pattern forming on the substrate during exposure. The records were stable under ambient conditions and offered sufficient contrast for transmission or reflection readout. This single-step simplicity and low cost motivated the subsequent holographic recording studies.

6.3 Holographic Recording by Photodeposition

The extension of LPPD to holographic recording was reported in 1992 in Papers [19, 22], co-authored with Weiss and Friesem. Holographic recording by photodeposition was achieved by exposing the a-Se hydrosol to the interference pattern formed by two coherent laser beams at 514 nm, intersecting at the substrate surface. The work showed that coherent, well-defined gratings could be recorded with diffraction efficiencies ~ 13%, sufficient for practical holographic applications, and that the spatial period of the gratings corresponded accurately to the interference fringe spacing predicted by the beam geometry. These results introduced photodeposition-based holographic recording within the broader class of inorganic holographic recording materials under investigation at the time.

6.4 Resolution Capabilities and Spatial Frequency Response

The resolution capabilities of LPPD holographic gratings were investigated systematically from 1994 onward in Papers [24, 25], co-authored with Weiss et al. Photodeposition was shown to faithfully record spatial frequencies of 1800 lines/mm, well within the regime relevant for holographic data storage and optical element fabrication. Importantly, the practical resolution limit was governed by the optical parameters of the system lenses rather than intrinsic limitations of the photodeposition process itself.

A transfer modulation function (MTF) for LPPD recording was developed [25] to relate frequency response to the microscopic parameters of the colloid system:

$$M(f) = \left[1 + \left(\frac{3\pi^2 n a^2 f}{\lambda_0}\right)^2\right]^{-1}$$

Here, f is the spatial frequency of the holographic grating, n is the colloid refractive index, a is the colloid particle radius, and λ_0 is the free-space recording wavelength. This model served as a quantitative design tool for applications which require precise spatial-frequency performance. Typical measurements yielded an MTF half-power point at 1500 lines/mm (corresponding to ~ 0.67 μm feature size), a peak corrected diffraction efficiency of 13% at 1100 lines/mm, and a practical resolution limit near 2200 lines/mm (~ 0.45 μm feature size) read out at 0.633 μm. The fact that the recorded grating period (0.45 μm) is finer than the readout wavelength (0.633 μm) underscores a key advantage of LPPD. Recording in the blue-green and reading in the red does not fundamentally compromise achievable spatial resolution.

6.5 Write/Erase Capabilities

This capacity for erasure and re-recording was investigated for LPPD in 1996 in Paper [31], The results showed that write/erase cycling of dots and line widths in the range of 0.5–20 μm was achieved through thermal or photo-induced redistribution of the deposited a-Se material. Fidelity after erasure was assessed by comparing the diffraction efficiency and spatial-frequency response of gratings recorded across successive write/erase cycles.

6.6 Inorganic Materials for Archival Holographic Recording

The archival potential of LPPD holographic recording was addressed in Paper [34], in 1997. That study comparatively assessed inorganic photodeposited materials, including a-Se and cadmium-based films for long-term holographic storage in terms of stability, sensitivity,

resolution, and dynamic range. By depositing inorganic films from a liquid-phase colloidal precursor under ambient conditions, LPPD offered archival-quality recording without the complexity of gelatin processing. This was supported by experimental data on accelerated aging, thermal stability, and diffraction efficiency retention. Together, these results completed a body of research spanning process demonstration [19, 22], resolution characterization [24, 25], reversibility [31], and archival assessment [34].

7. Photonics Applications II : Diffractive Optical Elements (2003–2005)

Studies reported in Papers [38], [39], and [42] demonstrated that LPPD can produce functional DOEs of practical quality from colloidal liquid-phase precursors under ambient conditions. The foundational work in 2003 [38], showed that optical elements, including grating structures, zone plates, and various symmetric focusing elements, could be fabricated by photodeposition from a-Se colloid solutions. Spatially structured illumination from photolithographic masks was used to define the element geometry. A complementary study [39] examined DOE writing via direct laser beam scanning. This replaced static masks with a focused raster beam steered across the substrate by a computer-controlled stage. The mask-based exposure offered higher throughput for mass-producing identical elements [38], while the direct-write approach provided design flexibility essential for prototyping and iteration [39]. By 2005, Paper [42] further evolved the process by utilizing computer-generated masks. Binary or grayscale amplitude patterns enabled the photodeposition of complex optical functions requiring the full generality of computer-generated holography (CGH) techniques.
Fig. 5 presents experimental photodeposition results on Mylar substrates using a white light source, originally produced in 1988 [15] with various masks. The images show: a test pattern bar chart with resolvable linewidths of 1–2 μm; an analogue image with varying grey levels; a recorded bit pattern with discrete spots of ~0.003 mm² area; and a transmission diffraction pattern from a photodeposited grating illuminated by a distant white point source.

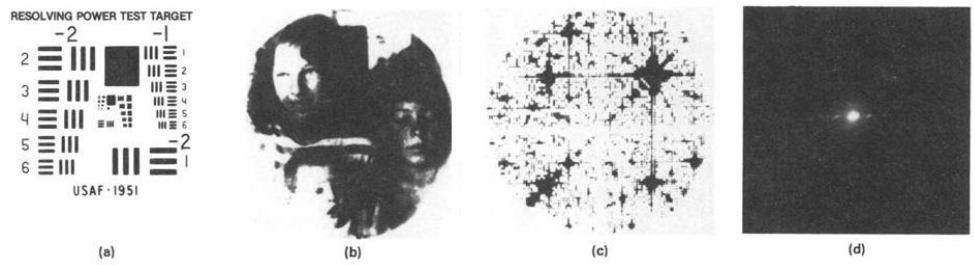

Fig. 5. Test patterns recorded as thin films (resolving power ~ 850 lp/mm): (a) Test target resolving chart; (b) recorded gray levels image; (c) Bit pattern; (d) Transmitted Diffraction Pattern

8. Pulsed Laser Photodeposition and Nanostructures (2003–2012)

8.1 Nanoscale Transition

The progression of LPPD research into the nanoscale domain was driven by two converging developments. The first was technological, with the increasing availability of pulsed laser sources [46], especially excimer lasers [45] operating in the ultraviolet. These offered nanosecond pulse durations and peak intensities orders of magnitude above those achievable with continuous-wave illumination. This opened new parameter regimes for faster

photodeposition. Within these regimes, the interaction between the laser pulse and the colloidal medium produced deposition dynamics qualitatively different from those observed under CW illumination. The second driver was the growing recognition, across materials science and photonics, that nanoscale structural features below 100 nm confer optical properties far superior to those of bulk or micron-scale materials.

8.2 CW vs. Pulsed Laser Photodeposition of a-Se Nanofilms

Continuous-wave (CW) Ar laser illumination (457 - 497 nm) in LPPD was first described in 1992 [21] as a controlled, monochromatic alternative to broadband sources. The approach exploited spatial coherence for precise beam shaping and interference, which also underpins holographic recording [19, 24–25]. The study mapped how wavelength, intensity, and exposure duration govern deposition rates and film morphology. In 2007, the focus shifted to pulsed laser photodeposition [45], using an ArF excimer laser (193 nm) with nanosecond pulses. This deep-ultraviolet excitation enabled efficient energy coupling and confined deposition to timescales shorter than thermal diffusion, improving resolution. ArF-pulsed films also showed better thickness uniformity and nanoscale surface smoothness, likely because each pulse triggered a discrete deposition event rather than the kinetically more complex process of the CW laser's continuous exposures. The pulsed method also revealed a critical fluence threshold for deposition, consistent with the photo-precipitation models developed in Papers [4, 5, 13].

8.3 Image Analysis by SEM and Advanced Evanescent Nanoscopic Characterization of Photodeposited Structures

Structural characterization of photodeposited a-Se films evolved through a series of complementary techniques. In 1995, Paper [29], co-authored with Baranauskas et al., applied scanning force microscopy (SFM) in contact mode to image surface topography at nanometric resolution. The SFM images revealed a morphology consistent with the films' colloidal origin. At lower doses, individual grains remained resolvable and the surface was comparatively non-compact. Higher doses produced denser, smoother films. This provided direct experimental support for the growth models of Papers [35] and [40], which attribute film structure to the statistical accumulation and cohesion of particles under local illumination. Paper [30], in 1996, extended the morphological analysis to laser-irradiated films using optical micrographs and SEM. Two quantitative methods were applied: 2D Fourier analysis for particle size distribution, and fractal dimensional analysis for structural compactness. These revealed that film disintegration during laser-induced ablation occurs reversibly - a behavior distinguishing photodeposited structures from vacuum deposited films.

In 2007, a collaboration with Mihailescu's group [44] introduced a non-contact evanescent optical method capable of probing nanoscopic profiles at nanometer depth scales. This showed that KrF laser photodeposition at 248 nm yields discrete deposits whose dimensions are precisely governed by pulse parameters and colloid concentration. Paper [46] introduced the Differential Evanescent Light Intensity (DELI) as a quantitative measure of growth rate and thickness profile evolution. Nanoscale kinetic data were obtained from scattered intensity comparisons before and after deposition, providing further experimental validation for the kinetic models of Papers [14] and [16]. The fundamental equation governing the normalized

evanescent scattering light parameter, $\eta = I_z(h)/I_0$ was derived in [49], then approximated successively to the zone where $\alpha h \ll 1$. It relates η to the local deposited thin film thickness $h(x, y)$ at any point (x, y) on a waveguide by the following equations:

$$\eta\big(h(x,y)\big) = \left(1 - e^{-\gamma h(x,y)}\right) \cdot e^{-\alpha h(x,y)} \sim \left(1 - e^{-\gamma h(x,y)}\right) \cdot e^{-\alpha h(x,y)} \sim \gamma h$$

where α is the film optical absorption constant, and γ is the material's specific extraction parameter, defined as the product of the material's constituent particle concentration N_a and their effective evanescent scattering cross-section σ_{ev}:

$$\gamma = N_a \sigma_{ev}$$

The final proportionality of $\eta\big(h(x,y)\big) \sim \gamma h$ to the local film thickness makes DELI a direct, simple quantitative probe of deposition profiles at the nanoscale. Grounded in electromagnetic modeling [49, 50], DELI was then validated across metallic, semiconducting, and dielectric systems [51], and subsequently extended to photodeposited bio-chromophore layers [52].

9. LPPD in the Broader Landscape of the Term "Photodeposition"

9.1 A Term with Multiple Lineages

The term photodeposition emerged empirically in 1976, at the Perakh laboratory (Hebrew University of Jerusalem) where collaborators conducted selenium chemical precipitation experiments in the dark. They accidentally discovered that illuminated colloidal hydrosols of amorphous selenium deposited thin solid films onto immersed insulating substrates. Because the effect seemed similar to electrodeposition, "Photodeposition" was adopted as a natural analogue. The systematic later usage of the term to describe a controlled surface process driven by photoexcitation of a colloidal liquid-phase precursor originated thus with the publications of Perakh et al. in 1976–1978 [1–5]. This predates the independent adoption of the photodeposition term also by the photocatalysis and semiconductor-processing communities.
Two earlier uses of related terminology exist, but neither established a lasting framework. Sadowsky and Payne (1958) [54] described light-assisted phosphor deposition driven by binder modification rather than particle photoexcitation. Clark and Vondjidis (1965) [55] observed photo-induced interactions between titanium dioxide and silver ions. This was later recognized as a precursor to photocatalytic metal deposition, though they did not frame it as photodeposition.
LPPD's scientific identity rests thus not only on its temporal priority but on a self-consistent body of knowledge spanning five decades of mechanism, kinetics, theory, and material generalization. Perakh and Peled's 1978 paper was extended by subsequent researchers to thin-film dynamics and silver halide composites [56], selenium photodeposition for nanostructured solar cells [57], and chemical solution deposition [58]. The 1997 LPPD previous review [33] likewise informed later on studies of chromium hydroxide kinetics and nickel-based nanostructured materials [59–61]. A 2007 review by Hugonnot and Delville [62] further confirms this lineage. They explicitly associate the early use of "photodeposition" with LPPD and its conceptual analogy to the electrodeposition paradigm.

9.2 The Photocatalysis Lineage: Kraeutler, Bard and Successors

A parallel lineage for the "photodeposition" term originates with Kraeutler and Bard [63], who in 1978 documented the photochemical deposition of platinum onto TiO_2 powder via UV excitation of the semiconductor. The resulting electron-hole pairs drive reduction of dissolved metal ions at the surface, depositing the metal directly onto the photocatalyst. This launched an extensive research program in photocatalytic metal deposition, later reviewed across a range of systems including metals such as Pt, Ag, and Pd deposited onto photocatalyst substrates such as TiO_2, ZnO, and CdS [64]. These photocatalytic processes differ from LPPD in fundamental ways. In photocatalysis, the semiconductor particle absorbs light and serves as the deposition substrate. In LPPD, light-absorbing colloidal precursor particles are the depositing species, settling onto a separate, transparent, insulating, non-photoactive substrate. Although the photocatalysis community adopted the term photodeposition independently and without reference to the LPPD literature, it has become one of the most widely used definitions of "photodeposition" in subsequent literature. The two fields share thus only the broad concept of light-driven deposition. They do not share the colloidal excitation mechanism, substrate material, thin-film geometry, or photonic devices fabrication focus that defines LPPD.

9.3 Photo-CVD and Related Methods

A further alternative use of "photodeposition" emerged in the semiconductor processing community during the 1980s, in the context of photo-CVD. Here, UV illumination from mercury lamps or excimer lasers photo-dissociates gaseous precursors to deposit thin films of semiconductors, dielectrics, or metals under milder conditions than thermal CVD. Several groups applied the term in this sense [65–67], including studies of silicon, dielectric, and III–V semiconductor films. Photo-CVD differs fundamentally from LPPD in both precursor phase and mechanism. It is an entirely gas-phase process. Light dissociates molecular gases rather than destabilizing a colloidal suspension, and film growth proceeds through surface reactions of photogenerated radicals rather than colloidal adhesion which governs LPPD. This usage reflects an increasing tendency over the years to apply the general "photodeposition" term to any light-driven deposition process, regardless of its physical phase or underlying mechanism.

9.4 Photo-Assisted Electrodeposition

A further use of a closely related terminology appears in light assisted electrodeposition, perhaps the closest to LPPD in its surface-process orientation. Here, illumination of a semiconductor electrode alters its electrochemical behavior, influencing the rate and selectivity of deposition from an ionic solution. Early studies [68, 69] exploited the photovoltaic effect at the semiconductor-electrolyte interface to drive preferential metal deposition. However, unlike LPPD, which acts through direct photoexcitation of a colloidal precursor, photo-assisted electrodeposition relies on light modifying the electronic state of a semiconducting electrode to facilitate ions reduction and deposition.

9.5 A Taxonomy of Photodeposition

The survey in Chapter 9 reveals a family of related but distinct processes united by light-driven material deposition. Table 1 organizes the principal photodeposition, photocatalytic, and

photo-assisted variants by precursor phase, driving mechanism, depositing species, and primary application domain.

Table 1. Taxonomy of photodeposition, photocatalytic and photo-assisted processes.

Process	Precursor Phase	Driving Mechanism	Depositing Species	Primary Applications
LPPD (Peled, 1976 -) [1, 2, 3–5]	Liquid colloidal	Photo-excited colloidal destabilization	Colloidal nanoparticles	Thin films, holography, DOEs, nanophotonics
Photocatalytic deposition (Kraeutler and Bard, 1978 -) [63]	Ionic solution	Charge-carrier mediated ion reduction	Metal ions → elemental metal	Photocatalysis, solar energy, antimicrobials
Photo-CVD (Solanki and Sato, (1980 -) [65-67]	Gas phase	Photodissociation of molecular precursors	Radical species	Semiconductor device fabrication
Photo-assisted electrodeposition (Kawamura, Chang 2006, 2014) [68-69]	Ionic solution	Photovoltaic effect at semiconductor electrode	Metal ions → elemental metal	Selective metal deposition, solar cells
Phosphor photodeposition (Sadowsky & Payne, 1958) [54]	Particle suspension	Photochemical binder modification	Phosphor particles	CRT screen manufacturing

Within this taxonomy, LPPD occupies a distinct position, not as superior or inferior to the alternatives, but as a specific approach employing a colloidal liquid-phase precursor, driven by photo-excited colloidal destabilization, and targeting the fabrication of compact thin films for photonics and optical elements.

10. Conclusions and Future Directions

10.1 A Summary of the Five-Decade Arc

The “photodeposition” process from hydrosols, later termed LPPD, was initiated in 1976 at the Hebrew University of Jerusalem, with the observation that colloidal suspensions of amorphous selenium could deposit coherent thin films onto immersed substrates under illumination [1]. This discovery was archived in the three-part Selor Process trilogy [3–5].

Over five decades, the LPPD program advanced through a programmed sequence of developments. Early kinetic characterization [4] and theoretical interpretation [5] were extended by photo-adsorption kinetic models [14, 16]. Later developments incorporated photon correlation spectroscopy [28], optical response theory for irradiated colloid systems [32], and stochastic simulations of thin-film growth [35, 40]. These collectively enhanced the understanding of light–matter interactions in colloidal systems. LPPD also expanded the process beyond the founding a-Se material to CdS [20], ZnS [27], and chlorophyll-based bio-chromophore solutions [36].

Photonic applications provided the first optical-recording demonstration [15]. They further demonstrated holographic grating fabrication [19, 22], resolution characterization [24, 25],

write/erase capability [31], and archival holographic recording [34]. They also enabled the fabrication of diffractive optical elements using mask-based [38], direct-write [39], and computer-generated holographic methods [42].
The process later moved into nanoscale fabrication and characterization. This transition was driven by pulsed laser excitation [45], evanescent optical analysis [44, 46–51], scanning force microscopy [29], and image analysis of laser-modified films [30]. Together, these advances established LPPD also as a nanoscale deposition process platform.

10.2 Open Questions and Future Directions

Future developments for LPPD span five possible directions. First, pulsed illumination and nonlinear deposition thresholds [44, 45] may enable better spatial confinement, improving the lateral LPPD resolution below the diffraction limit. Second, light-driven deposition of proteins or DNA-conjugated nanoparticles could advance bio-photonic and bio-inorganic hybrid devices, building on the previous bio-chromophore results [36, 41, 52]. Third, LPPD's ambient-condition capability [38, 39, 42] may allow patterning of active materials onto meta-surfaces and plasmonic arrays without vacuum processing. Fourth, its liquid-phase, ambient processing eliminating high-temperature steps and corrosive developers will align better with green chemistry principles [70, 71]. Finally, theoretical extensions into quantum colloidal photo-physics are needed to refine the current classical kinetic models [14, 16, 32, 35, 40] with frameworks incorporating quantum confinement effects.

References

[1] M Perakh, A. Peled, (1976). “Photodeposited Thin Se-Films”, Bulletin of the Israel Physical Society, Vol.*22*, p.87. (Presented at the Annual Meeting of the IPS, Technion, Israel Institute of Technology, Haifa, April 11–12, 1976).

[2] M Perakh, A. Peled, (1977). “Photodeposited Thin Se-Films of Amorphous Selenium. Journal of the Electrochemical Society”, *124*(3), 110C. (Abstract No. 110, 151st Meeting of the Electrochemical Society, Philadelphia, PA, May 8–13, 1977).

[3] M. Perakh, A. Peled, Z. Feit, "Photodeposition of a-Se Films by the Selor Process: Part I , Main Features of the Process, Film Structure”, Thin Solid Films, 50, 1978, pp. 273–283.

[4] M. Perakh, A. Peled, "Photodeposition of a-Se: Part II, Kinetics Studies", Thin Solid Films, 50, 1978, pp. 283–291.

[5] M. Perakh, A. Peled, "Photodeposition of a-Se: Part III, Interpretation of the Structural and Kinetics Studies", Thin Solid Films, 50, 1978, pp. 293–300.

[6] M. Perakh, A. Peled, "Light Temperature Interference Governing the Inverse and Combined Photoadsorption and Photodeposition of a-Se Films", Surface Science, 80, 1979, pp. 430–440.

[7] A. Peled, "Studies of a-Se Dispersions Used in the Photodeposition Process: Part I: Dispersion Properties in the Dark", Journal of Dispersion Science & Technology, 5 (2), 1984, pp. 219–226.

[8] A. Peled, "Volume Photodeposition Process in a-Se Hydrosols", Colloid and Polymer Science, 262, 1984, pp. 817–820.

[9] A. Peled, "Photodeposition Recording and Display Technology", Optical Engineering, 24 (4), 1985, pp. 717–718.

[10] A. Peled, M. Perakh, "Electrical and Photoelectrical Properties of Photodeposited a-Se Films", International Journal of Electronics, 58 (3), 1985, pp. 381–393.

[11] A. Peled, "Determination of Impurity Contents in the Photodeposition Process by X-Ray Fluorescence", Materials Chemistry & Physics, 13, 1985, pp. 483–487.

[12] A. Peled, "Optical Parameters of Photodeposited a-Se Films", Philosophical Magazine B, 54, 1986, pp. 171–177.

[13] A. Peled, D. Naot, "A Phenomenological Model of Photoprecipitation in a-Se Colloid Solutions", Colloid and Polymer Science, 265, 1987, pp. 986–992.

[14] A. Peled, M. Perakh, "On the Theory of Photoadsorption Kinetics of a-Se Colloids: A Simple Model for the Kinetic Parameters", Journal of Colloid and Interface Science, 122 (1), 1988, pp. 193–200.

[15] A. Peled, Y. Dror, "Optical Photorecording by the Surface Photodeposition Effect", Optical Engineering, 27 (6), 1988, pp. 482–485.

[16] A. Peled, D. Naot, M. Perakh, "On the Theory of Photoadsorption Kinetics of a-Se Colloids: The Thermal Activation Energy and Compensation Effect", Colloid and Polymer Science, 266, 1988, pp. 958–964.

[17] A. Peled, "Transformation Steps of Microstructures in Photodeposited Films of a-Se", Journal of Materials Research, 4 (1), 1989, pp. 177–179.

[18] A. Peled, E. Hadziioannou, "Thermal Characterization of a-Se Films Obtained by Low Temperature Photodeposition", Journal of Materials Science, 26, 1991, pp. 1769–1774.

[19] A. Peled, V. Weiss, D. Rosenblatt, A. A. Friesem, "Holographic Recording by Photodeposition Techniques", Optical Engineering, 31 (1), 1992, pp. 70–73.

[20] V. Weiss, A. Peled, A. A. Friesem, "Photodeposition of Thin Cd Films from CdS Colloid Solutions", Thin Solid Films, 218 (1), 1992, pp. 193–201.

[21] A. Peled, A. A. Friesem, K. Vinokur, "CW Laser Photodeposition of a-Se Films", Thin Solid Films, 218 (1), 1992, pp. 201–208.

[22] V. Weiss, A. Peled, A. A. Friesem, "Holographic Gratings Recorded by Photodeposition of Inorganic Colloids", SPIE Holographics International 92, 1732, 1992, pp. 131–136.

[23] A. Peled, N. Mirchin, "Photodeposition from Colloid Sols", Brazilian Journal of Vacuum Applications, 11 (1), 1992, pp. 104–112.

[24] A. Peled, V. Weiss, A. Shalgi, A. A. Friesem, "Resolution Capabilities of Photodeposited Holographic Gratings", Journal of Applied Surface Science, 79/80, 1994, pp. 393–398.

[25] V. Weiss, A. Peled, A. A. Friesem, "Spatial Frequency Response of Holographic Gratings Photodeposited from Inorganic Colloids", Applied Optics, 33 (22), 1994, pp. 4988–4992.

[26] A. Peled, "Photodeposition from Liquid Phase", SPIE ROMOPTO-94, 2461, 1995, pp. 82–94.

[27] A. Peled, B. Dragnea, R. Alexandrescu, A. Andrei, "Laser Induced Photodeposition from ZnS Colloid Solutions", Journal of Applied Surface Science, 86, 1995, pp. 538–542.

[28] N. Borochov, A. Peled, "Aggregation Kinetics of Photo-Excited Colloid Solutions Observed by Dynamic Photon Correlation Spectroscopy (PCS)", Journal of Applied Surface Science, 86, 1995, pp. 533–537.

[29] A. Peled, V. Baranauskas, C. Rodrigues, D. Art-Weisman, L. Grantman, A. A. Friesem, "Characterization of Photodeposited Selenium Planar Structures by Scanning Force Microscopy", Journal of Applied Physics, 77 (12), 1995, pp. 6208–6213.

[30] I. Lapsker, J. Azoulay, M. Rubnov, Z. Regev, R. C. Peled, A. Peled, "Image Analysis of Structural Changes in Laser Irradiated Thin Films of Photodeposited a-Se", Journal of Applied Surface Science, 106, 1996, pp. 316–320.

[31] A. Peled, L. Grantman, M. Ochayon, A. A. Friesem, "Investigations of Write/Erase Features by the Photodeposition Technique", Journal of Applied Surface Science, 106, 1996, pp. 306–310.

[32] N. Mirchin, A. Peled, "Theoretical Approach to Optical Response Properties of Photoprecipitation in Irradiated Colloid Systems", Journal of Applied Surface Science, 106, 1996, pp. 418–421.

[33] A. Peled, "Review: State of the Art in Liquid Phase Photodeposition Processes and Applications (LPPD)", Lasers in Engineering, 6, 1997, pp. 41–79.

[34] V. Weiss, A. A. Friesem, A. Peled, "Inorganic Materials for Archival Holographic Recording", Journal of Imaging Science and Technology, 41 (4), 1997, pp. 355–371.

[35] A. Peled, N. Mirchin, Z. Zacharia, C. R. Peled, "Simulation for Thin Film Growth Visualization in Photodeposition", Journal of Applied Surface Science, 154–155, 2000, pp. 324–330.

[36] A. Peled, Y. Dror, I. Baal-Zedaka, A. Porat, N. Mirchin, I. Lapsker, "Photobleaching and Photodeposition in a Chlorophyll Based Solution", Synthetic Metals, 115, 2000, pp. 167–171.

[37] A. Peled, N. Mirchin, "Liquid Phase Photodeposition Processes from Colloid Solutions", in Photo-Excited Processes, Diagnostics and Applications (PEPDA): Fundamentals, Applications and Advanced Topics, Chapter 9, Kluwer Academic Publishers, Netherlands, 2003, pp. 251–280.

[38] I. Baal-Zedaka, S. Hava, N. Mirchin, R. Margolin, M. Zagon, I. Lapsker, J. Azoulay, A. Z. Peled, "Photodeposition of Optical Elements from Colloid Solutions", Colloids and Surfaces A: Physicochemical and Engineering Aspects, 217, 2003, pp. 191–202.

[39] I. Baal-Zedaka, S. Hava, N. Mirchin, R. Margolin, M. Zagon, I. Lapsker, J. Azoulay, A. Peled, "Diffractive Optical Elements Written by Photodeposition", Journal of Applied Surface Science, 208–209, 2003, pp. 226–232.

[40] N. Mirchin, M. Sidi, Y. Muchnik, A. Peled, "Visualization Modeling of Thin Film Growth in Photodeposition Process", Journal of Applied Surface Science, 208–209, 2003, pp. 527–533.

[41] N. Mirchin, A. Peled, Y. Dror, "Modeling and Analysis of Bleaching Processes in Photo-Excited Chlorophyll Solutions", Synthetic Metals, 138, 2003, pp. 323–327.

[42] N. Mirchin, A. Peled, I. Baal-Zedaka, R. Margolin, M. Zagon, I. Lapsker, A. Verdyan, J. Azoulay, "Photodeposited Diffractive Optical Elements of Computer Generated Masks", Journal of Applied Surface Science, 248 (1–4), 2005, pp. 509–513.

[43] A. Peled, N. Mirchin, "Photo-Assisted Processes from Nano Size Colloid Sols", in J. J. Dubowski, S. Tanev (Eds.), Photon-based Nanoscience and Nanobiotechnology, NATO Science Series, Vol. 239, Springer, Netherlands, 2006, pp. 333–343.

[44] G. Socol, E. Axente, M. Oane, L. Voicu, A. Petris, V. Vlad, I. N. Mihailescu, N. Mirchin, R. Margolin, D. Naot, A. Peled, "Nanoscopic Photodeposited Structures Analyzed by an Evanescent Optical Method", Journal of Applied Surface Science, 253, 2007, pp. 6535–6538.

[45] A. P. Caricato, M. Martino, F. Romano, N. Mirchin, A. Peled, "Pulsed Laser Photodeposition of a-Se Nanofilms by ArF Laser", Journal of Applied Surface Science, 253, 2007, pp. 6517–6521.

[46] G. Socol, E. Axente, M. Oane, L. Voicu, A. Dinescu, A. Petris, V. Vlad, I. N. Mihailescu, N. Mirchin, R. Margolin, D. Naot, A. Peled, "Using Differential Evanescent Light Intensity for Evaluating Profiles and Growth Rates in KrF Laser Photodeposited Nanostructures", Journal of Materials Science: Materials in Electronics, 18, 2007, pp. 207–212.

[47] S. Aaronov, E. Ganon, P. Okhman, N. Mirchin, S. A. Popescu, I. Lapsker, A. Peled, "Differential Evanescent Light Intensity Evaluation of a-Se Nanostructure", Journal of Optoelectronics and Advanced Materials – Rapid Communications, 2 (1), 2008, pp. 614–617.

[48] S. Aaronov, E. Ganon, P. Okhman, M. Gankin, N. Mirchin, S. A. Popescu, I. Lapsker, A. Peled, "Evaluation of a-Se Nanostructure Morphology by Differential Evanescent Light Imaging", Journal of Nanophotonics, 3 (1), 2009, p. 031785.

[49] S. A. Popescu, B. Apter, N. Mirchin, I. Lapsker, A. Peled, "Differential Evanescent Light Intensity Imaging of Nanothin a-Se Dielectric Films and Simulation of Evanescent Waves", Journal of Advanced Research in Physics, 1 (1), 2010, p. 011010.

[50] M. Gankin, S. A. Popescu, B. Apter, N. Mirchin, I. Lapsker, A. Peled, "Differential Evanescent Light Intensity Imaging of Nanothin Films: Simulation of the Scattered Field", Physica Status Solidi C, 8 (9), 2011, pp. 2957–2960.

[51] N. Mirchin, B. Apter, I. Lapsker, V. Fogel, U. Gorodetsky, S. A. Popescu, A. Peled, G. Popescu-Pelin, G. Dorcioman, L. Duta, A. Popescu, I. N. Mihailescu, "Measuring Nanolayer Profiles of Various Materials by Evanescent Light Technique", Journal of Nanoscience and Nanotechnology, 12 (3), 2012, pp. 2668–2671.

[52] A. Peled, S. A. Popescu, "Nanometric z-Profiling of Bio-Chromophore Layers by DRLS", Acta Physica Polonica A, 137 (6), 2020, pp. 1163–1167.

[53] A. Peled, L. B. Schein, "The Thermal Activation Compensation Effect and the lsokinetic Temperature Relation to Physical Models", Physica Scripta., 44, 1991, pp. 304-309.

[54] M. Sadowsky, P. D. Payne, "Photodeposition of Luminescent Screens", Journal of The Electrochemical Society, 105 (2), 1958, pp. 105–107.

[55] W. C. Clark, A. G. Vondjidis, "An Infrared Study of the Photocatalytic Reaction Between Titanium Dioxide and Silver Nitrate", Journal of Catalysis, 4 (6), 1965, pp. 691–696.

[56] G. Hodes, G. Calzaferri, "Chemical Solution Deposition of Silver Halide Films", Advanced Functional Materials, 12 (8), 2002, pp. 501–505.

[57] X. Wang, H. Liu, W. Shen, "Controllable in situ photo-assisted chemical deposition of CdSe quantum dots on ZnO/CdS nanorod arrays and its photovoltaic application", Nanotechnology, 27 (8), 2016, 085605.

[58] G. Hodes, Chemical Solution Deposition of Semiconductor Films, Marcel Dekker, New York, 2002.

[59] E. Hugonnot, J.-P. Delville, "Kinetic control of periodic surface patterning by laser photochemical deposition", Applied Surface Science, 248, 2005, pp. 185–189.

[60] E. Hugonnot, X. Müller, J.-P. Delville, "Late-stage kinetics of laser-induced photochemical deposition in liquid solutions", *Journal of Applied Physics*, 92 (9), 2002, pp. 5520–5524.

[61] S. Giuffrida, G. G. Condorelli, L. L. Costanzo, G. Ventimiglia, R. Lo Nigro, M. Favazza, E. Votrico, C. Bongiorno, I. L. Fragalà, "Nickel nanostructured materials from liquid phase photodeposition", Journal of Nanoparticle Research, 9, 2007, pp. 611–619.

[62] E. Hugonnot, M-H. Delville, J-P Delville, "Universal behavior of photochemical deposition in liquid solutions driven by a one-photon transition", Physical Review E: Statistical, Nonlinear, and Soft Matter Physics, American Physical Society, 2007, 75 (6), pp.061602/1-12.

[63] B. Kraeutler, A.J. Bard "Heterogeneous photocatalytic preparation of supported catalysts. Photodeposition of platinum on titanium dioxide powder and other substrates", Journal of the American Chemical Society, 100 (13), 1978, pp. 4317–4318.

[64] K. Wenderich, G. Mul, "Methods, Mechanism, and Applications of Photodeposition in Photocatalysis: A Review", Chem. Rev., 2016, 116 (23), pp. 14587–14619

[65] R. Solanki, W. H. Ritchie, G. J. Collins, "Photodeposition of Aluminum Oxide and Aluminum Thin Films", Applied Physics Letters, 43 (5), 1983, pp. 454–456.

[66] S. Sato, A. Sobczynski, J.M. White, A.J. Bard, A. Campion, M.A. Fox, T.E. Mallouk, S.E. Webber, "Photochemical properties of ultrathin TiO_2 films prepared by chemical vapor deposition", Journal of Photochemistry and Photobiology A: Chemistry, 50 (2), 1989, pp. 283-290.

[67] Y. I. Nissim, J. M. Moison, F. Houzay, F. Lebland, C. Licoppe, M. Bensoussan, "Photo-assisted Deposition of Thin Films on III–V Semiconductors with UV and IR Lamps", Applied Surface Science, 46 (1–4), 1990, pp. 175–188.

[68] Y. Kawamura, T. Sakka, Y. Ogata, "Illumination-Modulated Electrodeposition of Various Kinds of Noble Metal on p-Type Silicon", Electrochemistry, 74 (7), 2006, pp. 544–548.

[69] T. W. Chang, W. H. Lee, Y. H. Su, Y. J. Hsiao, "Effects of photo-assisted electrodeposition on CuInSe2 thin films", Nanoscale Research Letters, 9 (1), 2014, p.660.

[70] B. Ruiz-Camacho, M. A. Valenzuela, J. A. Perez-Galindo, F. Pola, M. Miki-Yoshida, N. Alonso-Vante, R. G. Gonzalez-Huerta, "Oxygen Reduction Reaction on Pt/C Catalysts Prepared by Impregnation and Liquid Phase Photo-Deposition", Journal of New Materials for Electrochemical Systems, 13, 2010, pp. 183–189.

[71] A. A. Ryan, M. O. Senge, "How Green is Green Chemistry? Chlorophylls as a Bioresource from Biorefineries and their Commercial Potential in Medicine and Photovoltaics",Photochemical & Photobiological Sciences, 2014, pp. 1–20.